Deep-Sea Research I 57 (2010) 771–784

Contents lists available at ScienceDirect

Deep-Sea Research I

journal homepage: www.elsevier.com/locate/dsri

High resolution profiles of vertical particulate organic matter export off Cape Blanc, Mauritania: Degradation processes and ballasting effects

Morten Hvitfeldt Iversen [a,b,*], Nicolas Nowald [b], Helle Ploug [a,d], George A. Jackson [c], Gerhard Fischer [b]

[a] Alfred Wegener Institute for Polar and Marine Research, Am Handelshafen 12, D-27570 Bremerhaven, Germany
[b] University of Bremen, Department of Geosciences, Klagenfurterstrasse, Marum, Leobener Strasse, 28359 Bremen, Germany
[c] Department of Oceanography, Texas A&M University, College Station, TX 77843, USA
[d] Stockholm University, Department of Botany, Lilla Frescativägen 5, 10691 Stockholm, Sweden

ARTICLE INFO

Article history:
Received 26 February 2009
Received in revised form
12 March 2010
Accepted 24 March 2010
Available online 31 March 2010

Keywords:
Marine snow
Fluxes
Sinking velocity
Particle size spectrum
Flux feeding
Degradation

ABSTRACT

Vertical carbon fluxes between the surface and 2500 m depth were estimated from *in situ* profiles of particle size distributions and abundances me/asured off Cape Blanc (Mauritania) related to deep ocean sediment traps. Vertical mass fluxes off Cape Blanc were significantly higher than recent global estimates in the open ocean. The aggregates off Cape Blanc contained high amounts of ballast material due to the presence of coccoliths and fine-grained dust from the Sahara desert, leading to a dominance of small and fast-settling aggregates. The largest changes in vertical fluxes were observed in the surface waters (<250 m), and, thus, showing this site to be the most important zone for aggregate formation and degradation. The degradation length scale (L), i.e. the fractional degradation of aggregates per meter settled, was estimated from vertical fluxes derived from the particle size distribution through the water column. This was compared with fractional remineralization rate of aggregates per meter settled derived from direct ship-board measurements of sinking velocity and small-scale O_2 fluxes to aggregates measured by micro-sensors. Microbial respiration by attached bacteria alone could not explain the degradation of organic matter in the upper ocean. Instead, flux feeding from zooplankton organisms was indicated as the dominant degradation process of aggregated carbon in the surface ocean. Below the surface ocean, microbes became more important for the degradation as zooplankton was rare at these depths.

1. Introduction

A significant fraction of organic carbon produced by photosynthesis in the surface ocean is transported to deeper depths in the form of large sinking aggregates and fecal pellets (Fowler and Knauer, 1986). This transfer of carbon from the surface ocean to the deep ocean is termed "the biological carbon pump". In order to predict the efficiency of the biological carbon pump in time and space it is important to understand the mechanisms controlling the export of particulate organic carbon (POC) from the euphotic zone to the mesopelagic and deep ocean (e.g. Boyd and Trull, 2007; Buesseler et al., 2007b). The efficiency of the biological pump is determined by the remineralization rate and sinking speed of aggregated POC, where high remineralization rate prevents export while high sinking speed governs it.

Vertical profiles of particulate organic carbon (POC) show rapid declining carbon fluxes in the upper ocean (Martin et al., 1987; Schlitzer, 2000; Suess, 1980), indicating that controlling mechanisms for the efficiency of the biological pump take place in the surface ocean. However, measurements of aggregate processes and POC fluxes at these depths are difficult due to the fragile nature of large marine aggregates (marine snow), which makes them very difficult to collect and study. Further, standard sediment traps are bound to high uncertainties in the upper ocean and they can be used only to estimate the total flux because they average over all sizes and numbers of sinking particles (Buesseler et al., 2007a). The collected material by sediment traps can be altered by high concentrations of swimmers grazing on the collected material and by hydrolysis of the organic matter within the sediment trap. Problems of estimating size distribution and abundance of the aggregates have partly been overcome by the use of polyacrylamide gel in sediment trap collectors (Jannasch et al., 1980; Kiørboe et al., 1994; Waite and Nodder, 2001) and by the use of *in situ* camera systems (Asper, 1987; Gorsky et al., 1992; Nowald et al., 2006). The use of *in situ* camera systems has enabled measurements of high resolution depth profiles of aggregate size distribution and abundances for the whole water column. However, neither of these approaches can provide detailed information on chemical composition or remineralization

* Corresponding author at: University of Bremen, Department of Geosciences, Klagenfurterstrasse, Marum, Leobener Strasse, 28359 Bremen, Germany.
E-mail address: morten.iversen@uni-bremen.de (M.H. Iversen).

0967-0637/$ - see front matter © 2010 Elsevier Ltd. All rights reserved.
doi:10.1016/j.dsr.2010.03.007

rates of the aggregates, which are also needed to understand the processes controlling the biological pump.

Recent studies have combined the use of sediment traps and high resolution vertical profiles of aggregate size distribution and abundances to estimate relationships between physical properties and sizes of aggregates (e.g. Guidi et al., 2008b; Stemmann et al., 2002). Models have been based on the combination of trap fluxes and *in situ* camera profiles to investigate the role of physical coagulation, microbial activity, and zooplankton grazing (Stemmann et al., 2004a, 2004b), and to identify special flux patterns and the importance of different abiotic and biotic factors on export flux (Guidi et al., 2008a).

Most of the carbon remineralization takes place in the upper ocean, but varies considerably across the global ocean (Buesseler et al., 2007a; Martin et al., 1987; Suess, 1980). This high degradation of POC in the upper ocean has been suggested to be due to high ecto-enzymatic hydrolysis rates by aggregate attached bacteria (e.g. Smith et al., 1992) and respiration (Ploug et al., 1999), and from fragmentation and consumption of the aggregates by mesozooplankton (Dilling and Alldredge, 2000; Kiørboe, 2000; Steinberg, 1995). These degradation processes convert the POC into CO_2 and dissolved organic carbon (DOC), and convert the large, sinking aggregates into smaller aggregates with reduced sinking speeds. However, the relative importance from the different degradation processes of the aggregated POC in the upper ocean is still unclear.

The aim of the present study was to identify regulating processes for the export fluxes off NW Africa (Cape Blanc, Mauritania) and to identify important degradation processes in the upper ocean. For the first time, direct measurements of settling velocities and carbon degradation on aggregates were combined with high resolution vertical fluxes derived from deep ocean sediment traps and *in situ* camera system profiles. We estimated vertical carbon fluxes through the water column between the ocean surface and 2500 m depth using particle size distributions determined by an *in situ* camera system in combination with sediment trap flux-determined size-specific relationships of aggregate mass and sinking velocity. We compared fluxes estimated using a locally derived relationship for size-specific aggregate mass and sinking velocity against fluxes estimated using a global derived size-specific relationship to evaluate the importance of aggregate composition on fluxes. The aggregation potential of organic matter was investigated by incubation water samples in roller tanks, and measured size-specific O_2 uptake, sinking velocity, and composition of the formed aggregates.

2. Material and methods

2.1. Field sampling

We collected data on vertical particle size distribution, vertical fluxes, and hydrology during a cruise from the 23rd to the 29th of March 2007, aboard the German RV Maria S. Merian (leg 04/4b). This study was conducted in the region off Cape Blanc (Mauritania) and located within the Canary Current (CC; Fig. 1), which is the second most productive of the Eastern Boundary Upwelling Systems (Carr, 2002). The strongest upwelling is located off Cape Blanc (~21°N), where southward flowing North Atlantic Central Water (NACW) meets the less saline and nutrient-rich northward flowing South Atlantic Central Water (SACW; Hughes and Barton, 1974).

The Particle Camera (ParCa; Ratmeyer and Wefer, 1996) was deployed four times during the cruise (Table 1), and obtained an image for every 10 m between the surface and 2500 m depth. The

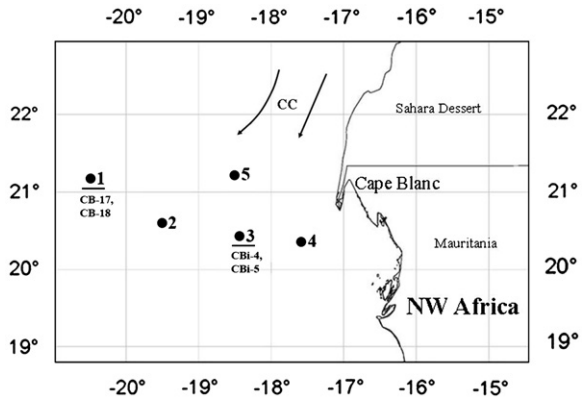

Fig. 1. *Location of the sample stations*. Five stations were sampled during RV Merian cruise 04/4b off Cape Blanc, NW Africa (Mauritania). The closed circles indicate the position of each station number (see Table 1). Vertical profiles of particle size distribution and abundance were obtained at Stations 1–4. The underlined stations indicate the position of deep ocean sediment trap sites CB and CBi positioned at Stations 1 and 3, respectively (see Tables 1 and 2). Aggregation potential was investigated at Stations 1, 2, 4, and 5 (see Table 1). The arrows indicate the Canary Current flow (CC).

ParCa was an improved version of the system used in Nowald et al. (2006). It consisted of a NIKON Coolpix 995 still image camera (3.34 megapixel) with micro-controller and software useable at depths <4000 m. A collimated light source (strobe) mounted perpendicular to the camera view illuminated a volume of 12.4 L (12 cm width). The *in situ* depth was transmitted by a SeaBird 19 CTD to the camera, creating an image every 10 m, while descending at 0.3 m s^{-1}. The ParCa was deployed only during night to prevent interference by ambient light.

CTD data on salinity, temperature, and fluorescence were obtained simultaneously with the ParCa data using a SeaBird 19 CTD equipped with a CHELSEA fluorometer. Water for measurements of particulate organic and inorganic carbon, dry weight of suspended particles, aggregate potential, and particle identification was collected with a CTD rosette equipped with 12×12-L Niskin bottles.

The vertical mass flux was captured by two large-aperture time-series deep ocean sediment traps of the Kiel type with a cup opening of 0.5 m^2. There were traps at ~1200 m for Station 1 (CB-17, CB-18) and at ~1200 and ~1800 m depth for Station 3 (CBi-4, CBi-5; Table 2). We collected the mass fluxes, before and after the ParCa deployment (Tables 1 and 2). Before sediment trap deployment, the cups were filled with filtered seawater with a salinity of 40 and poisoned with $HgCl_2$. The collected material was carefully wet-sieved through 1 mm nylon mesh to remove swimmers. The >1 mm size fraction contained only a few crustaceans and no large particles. Particle flux data therefore refer to the <1 mm size fraction, which also included fragile material settling as large aggregates before being disrupted in the trap or during subsequent handling (Fischer and Wefer, 1991). The homogenized samples were split into sub-samples for further analysis. Total carbon, organic carbon, and nitrogen were obtained by combustion on a HEREAUS-CHN analyzer. Organic carbon was measured after removal of carbonate with 2 N HCl. Carbonate was determined by subtracting organic carbon from total carbon, the latter being measured by combustion without a pre-treatment with 2 N HCl.

2.2. Vertical particle abundance and size distribution

The ParCa recorded and provided realistic information on abundance, size, and shape of objects within the size range 0.15–6.5 mm, with the lower bound set by optical limitation and

Table 1
Physiochemical parameters and experiments for each station sampled.

Station number	Station name [longitude, latitude]	*F*-max depth (m)	Temperature (°C)	Salinity (psu)	Experiments
1	**GeoB-11833** **Trap site CB-17 & CB-18** **[21°17.170N, 20°48.223W]**	48	20.4	36.6	Agg. potential (N=17) – ParCa
2	**GeoB-11834** **–** **[20°59.989N, 19°50.014W]**	35	20	36.5	Agg. potential (N=18) POC ParCa
3	**GeoB-11835** **Trap site CBi-4 & CBi-5** **[20°44.796N, 18°42.021W]**	20	18.3	36.1	– POC ParCa
4	**GeoB-11836** **–** **[20°34.969N, 17°58.761W]**	25	18	36.1	Agg. potential (N=18) POC ParCa
5	**GeoB-11839** **–** **[21°19.997N, 18°50.475W]**	25	19.1	36.5	Agg. potential (N=16) POC ParCa

Depth of fluorescence maximum (*F*-max depth [m]), *in situ* temperature, *in situ* salinity, and experiments performed for different stations; aggregation potential (Agg. potential), number of measured aggregates from the aggregation potential incubations (N), determination of particulate organic carbon content of seawater samples collected from *F*-max (POC), vertical profiles of particles of size between 150 μm and 6.5 mm (ParCa).

Table 2
Trap identifier, trap depth, collection periods, and total mass and organic carbon fluxes shown for each deployment.

Station number (trap name)	Trap depth (m)	Begin (date)	End (date)	Mass flux ($mg\,m^{-2}\,d^{-1}$)	Organic carbon flux ($mg\,C\,m^{-2}\,d^{-1}$)
Station 1					
CB-17	1204	15.03.07	23.03.07	218.7	8.02
CB-18	1222	25.03.07	10.04.07	236.2	13.9
Station 3					
CBi-4 upper	1256	15.03.07	23.03.07	1046.4	76.8
CBi-4 lower	1866	15.03.07	23.03.07	1713.4	111.7
CBi-5	1263	28.03.07	03.04.07	486.5	31.3

the upper bound by low concentrations of the large aggregates. The recorded images were analyzed using the image analyze software "Optimas" (Media Cybernetics). The software recognizes foreground objects (particles) below a given threshold value, returning the area within an outer perimeter and abundance of each aggregates in an image. The area of each particle on the image profile was converted to equivalent spherical diameter (ESD, mm) and equivalent spherical volume (ESV, mm^3). We excluded zooplankton from the profiles by visually investigating every image containing particles >1 mm and excluding every identified zooplankton organisms from the returned data. No large stringers or comet shaped aggregates were observed during the visual investigations. Each image was calibrated against a scale included in an image before and after the obtained profile.

We divided each profile vertically into 54 layers, by having 10 m thick layers in the upper 50 m and 50 m thick layers at depths below 50 m. For each layer we divided particle sizes into 17 classes, and then calculated the particle size spectrum n as a function of diameter (d) by dividing the concentration of particles (ΔC) in a given small size range (Δd): $n=\Delta C/\Delta d$. When fitting the size spectrum to a relationship of the type $n=kd^{-b}$, the constant k depends on the concentration of particles and b describes their distribution with size. Larger values of b describe steeper slopes of the curve when $\log(n)$ is plotted as a function of $\log(d)$. Flux estimations were made using the particle size spectra in each depth layer (see Section 2.3).

2.3. Flux estimations from particle abundance and size

We calculated the mass flux from the particle size spectra using the method described in details in Guidi et al. (2008b). They assumed that the total mass flux (F) is the mass flux spectrum integrated over all particle sizes. When the diameter (d) is used as a measure for particle size, we get

$$F=\int_0^{\infty} n(d)m(d)w(d)d(d) \quad (1)$$

where $m(d)$ is the mass of an individual particle of diameter (d), and $w(d)$ is its sinking velocity. Often both particle mass (m) and sinking velocity (w) are expressed by power relationships ($y=ax^b$) as a function of particle diameter d (e.g. Alldredge and Gotschalk, 1988). Therefore, their combined quantity can be described as

$$wm=Ad^B \quad (2)$$

If the size distribution of the aggregates and the value of A and B are known, the mass flux can be calculated from the particle size spectra using Eqs. (1) and (2). However, the values of A and B are unknown. We therefore followed the method of Guidi et al. (2008b) and used a minimization procedure to find the A and B values that provided the best fit between fluxes collected with the deep ocean sediment traps and fluxes calculated from the particle size distributions obtained at the same depth and station as the trap flux. The MatLab function *fminsearch* (The Mathworks, Inc., Natick, MA) was used to find the A and B value of Eq. (2) that minimized the log-transformed differences (ΔF_c) between sediment trap ($F_{T,i}$) and size spectrum estimated fluxes ($F_{E,i}$) based on Eq. (1) (Guidi et al., 2008b):

$$\Delta F_C=\sum_i[\log(F_{E,i})-\log(F_{T,i})]^2 \quad (3)$$

The logarithmic transformation ensures equal weight to the differences for small and large fluxes. The minimization procedure yields only one pair of A and B values (Table 3). Thus, it is assumed that mass and sinking velocity as a function of particle size are constant for all depths (Eq. (2)).

Table 3
Coefficient (A) and exponent (B) of the empirical relationship between the aggregate size and the related mass and particulate organic carbon (POC) fluxes Eq. (2) determined by minimization of the flux estimations by the particle camera (ParCa) and the deep ocean sediment trap measurements.

Study	Fluxes	A	B	R^2
This study	Mass	1396.9	3.65	0.85
This study	POC	273.8	4.27	0.74
Guidi et al. (2008b)	Mass	109.5	3.52	0.70
Guidi et al. (2008b)	POC	12.5	3.81	0.73

The A and B values from Guidi et al. (2008b) are determined by minimization of 118 global camera profiles and trap measurements. The A and B values for this study are determined by minimization of 5 local camera profiles and trap measurements. R^2 indicates the correlation coefficient obtained from the fit between the sediment trap flux and the estimated flux using the found A and B values.

The A and B values from Guidi et al. (2008b) were used to estimate fluxes based on Eqs. (1) and (2), to compare the ability of global (Guidi et al., 2008b) and regional (our results) derived data sets to match the measured fluxes (Table 3). The A and B values from Guidi et al. (2008b) were derived from underwater video profiles and sediment trap deployments in the Mediterranean Sea, Pacific, and North Atlantic.

2.4. Aggregation potential

The tendency of *in situ* materials (particulate organic and inorganic materials) to form aggregates was assessed by following the aggregate formation of suspended material in water samples from the fluorescence maximum. The fluorescence maximum was identified using chlorophyl fluorescence sensors on a CTD-SBE 19. Water samples were collected at four stations (1, 2, 4, and 5), and incubated in ten 1.15 L Plexiglas cylinders (roller tanks) of diameter 14 cm and depth 7.47 cm. The filled roller tanks were rotated at 3 rotations per minute (rpm) on a rolling table at *in situ* temperature (20 ± 1 °C) in dim light (Shanks and Edmondson, 1989). The formation of aggregates within the roller tanks was followed during 18 h incubations. To obtain a quantitative measure for the aggregation potential of different components of the suspended particles we measured phytoplankton concentrations, the particulate organic carbon (POC) content, dry weight of particles, and particle composition in the water samples before incubation and within the aggregates formed during the incubation.

2.5. Scanning electron microscopy

The particle composition in the water before the incubations and in the aggregates formed during incubations was assayed and examined visually using a scanning electron microscope (SEM). Water samples and aggregates were filtered onto 0.4 μm polycarbonate filters, rinsed with milliQ water, and dried >24 h at 40 °C. The filters were covered with a 5 nm gold–palladium layer (SC500, Emscope) before magnification in the SEM (FEI Quanta 200F with xTmicroscope software). Random areas on each filter were chosen for visual quantification and identification of the content.

2.6. Particulate organic carbon and dry mass

POC content and dry weight of suspended material from the fluorescence maximum were measured from five replicates of 2.5 L water filtered through pre-combusted (450 °C, 12 h) and pre-weighed Whatman GF/F filters (diameter: 25 mm) at each station (Table 1); 2.5 L milliQ water was filtered through three filters and used as blanks. Before determination of the carbon content, the filters were dried at 40 °C (>48 h) and re-weighed to determine dry weight of the suspended material. To remove inorganic carbon all filters were fumed in hydrochloric acid (HCl) before carbon analyses were performed on a EuroEA 3000 CN Element Analyzer.

After aggregation 2–5 aggregates with known and similar volumes were filtered onto pre-weighed 0.45 μm, 25 mm silver filters (Millipore, Bedford). The filters were gently rinsed with de-ionized water, and dried at 40 °C (>48 h) before being re-weighed on a Mettler Toledo UMX2 balance (sensitivity: 0.1 μg). The total particulate organic carbon (POC) content of the aggregates was then measured with an EA mass spectrometer (ANCA-SL 20-20, Sercon Ltd. Crewe, UK) having a precision of ± 0.7 μg C, or 0.3%. Half of the filters (total of 15 filters) were fumed with hydrochloric acid (HCl) before the POC measurements. The difference in POC content between the fumed and non-fumed samples was used to determine the inorganic carbon content. The POC content of each aggregate was assumed to equal its volume fraction times the total POC determined for the filter.

2.7. Size and sinking velocity of aggregates

Size-specific sinking velocity of individual aggregates was measured in a vertical flow system (Ploug and Jørgensen, 1999). Individual aggregates were gently transferred from the roller tanks to the open flow-through chamber using a wide bore pipette. The flow chamber was a 10 cm high Plexiglas tube of 5 cm diameter with a net extended in the middle. The net created a relative uniform laminar flow field across the upper chamber when a flow was supplied from below (Ploug and Jørgensen, 1999; Ploug et al., accepted for publication). The flow was adjusted with a needle valve until the aggregate was suspended one diameter above the net, where its sinking velocity was balanced by the upward-directed flow velocity. The sinking velocity of an aggregate was calculated by dividing the flow rate by the cross-sectional area of the flow chamber at that point. Triplicate measurements of sinking velocity were made for each aggregate. The length of all three aggregate axes (x, y, and z directions) was measured in the flow system using a horizontal dissection microscope with a calibrated ocular. The aggregate volume was calculated by assuming an ellipsoid shape. For comparison with other aggregate shapes we calculated the equivalent spherical diameter (ESD) of a sphere with equivalent volume as that of the ellipsoid.

2.8. Microbial respiration rates on aggregates

Oxygen concentration gradients at the aggregate–water interface were measured at 50 μm resolution in darkness at steady state using a Clark-type oxygen micro-electrode with a guard cathode (Revsbech, 1989). The micro-electrode was calibrated in air-saturated and in anoxic seawater. The electrode current was measured by a pico-ampere meter (Unisense, PA2000) connected to a strip chart recorder (Kipp and Zonen). The tip of the micro-electrode was 2 μm wide and was moved gently towards the surface of the aggregate. The aggregates appeared highly porous and we could not detect significant oxygen gradients when they were suspended in the flow field. Oxygen distributions were therefore measured at stagnant conditions at *in situ* temperature in darkness to avoid underestimation of O_2 respiration due to advection through the aggregates (Ploug et al., 2002). To avoid any limitation in oxygen supply due to wall effects, we placed

single aggregates on the net in the flow chamber while measuring oxygen distributions (Ploug and Jørgensen, 1999). The O_2 concentration within aggregates was $>90\ \mu M$ during measurements, and respiration was thus not diffusion-limited by O_2. Oxygen flux was calculated from the measured oxygen gradient at the aggregate–water interface (Ploug et al., 1997). We used a temperature and salinity corrected oxygen diffusion coefficient of $1.95 \times 10^{-5}\ cm^2\ s^{-1}$ in the calculations. The surface area of the aggregates was calculated according to Maas (1994), and used to calculate area-integrated oxygen fluxes. Carbon respiration rates were calculated assuming a respiratory quotient of 1.2 mol O_2 to 1 mol CO_2. No zooplankton organisms were present during the respiration measurements, and, thus, the measurements include respiration by live phytoplankton cells, attached bacteria, and protozoa and not respiration from zooplankton on aggregates or zooplankton consuming whole particles (flux feeding).

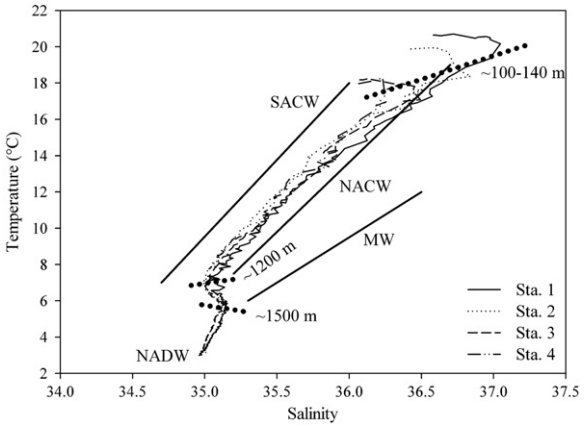

Fig. 2. *Temperature–salinity plot.* Temperature plotted against salinity for the four stations where vertical particle size distributions were measured (Stations 1–4). The dotted lines indicate depths of the profiles. The solid lines indicate different water masses: South Atlantic Central Water (SACW), North Atlantic Central Water (NACW), Mediterranean Water (MW), and North Atlantic Deep Water (NADW).

3. Results

3.1. Hydrological conditions

Our study site, located between 21.2°N and 20.3°N, was in a major upwelling region (Wooster and Reid, 1963) with offshore Ekman transport governing high open ocean primary production and occurrence of coastal phytoplankton several hundred kilometres offshore (Van Camp et al., 1991). Giant Cape Blanc filaments spread high pigment concentrations <450 km offshore in a region that includes our stations (Fig. 1). Our cruise was during the intense spring upwelling season (Mittelstaedt, 1991; Van Camp et al., 1991) which is also a time of high dust supply from the Sahara region (Bory and Newton, 2000; Van Camp et al., 1991). The salinity and temperature distributions that we observed indicate that there was high coastal upwelling of cold and less saline SACW and strong offshore Ekman transport during our cruise (Fig. 2). The increased salinity and temperature in the surface waters at the offshore stations (Stations 1 and 2) resulted from mixing of this upwelled water with the more saline and warmer NACW. Below ~140 m the strong influence by the upwelled SACW had declined and water layer persisted, with slightly stronger influence from NACW at the offshore station (Fig. 2). The salinity increase observed at ~1200 m depth was due to mixing with high saline Mediterranian water (MW) (Hughes and Barton, 1974). Below 1500 m all stations showed a decrease in salinity and temperature approaching those of North Atlantic Deep Water (NADW; Hughes and Barton, 1974; Fig. 2).

3.2. Vertical particle profiles

Maximum particle concentrations occurred in the surface water <80 m depth for all profiles (Fig. 3A). The maximum particle concentration at the surface decreased with increasing distance from the coast: 80–100 particles L^{-1} at Stations 3 and 4 (coastal sites), and ~30 particles L^{-1} at Stations 1 and 2 (open ocean sites). All profiles showed non-prominent subsurface particle increases. This was at ~300 m depth for the coastal sites and at 500–600 m for the open ocean sites. This particle increase was due to an increase in the small particles (0.15–0.5 mm ESD). The vertical region with elevated particle abundances around the subsurface particle increase became thicker with increasing distance from the coast. The largest extent of this feature was between 180 and 880 m depth at Station 1. At Station 3 particle concentrations increased from 1500 m to the bottom of the profile at 2500 m (Fig. 3A). The two coastal stations had approximately three times higher particle abundances at all depths than the open ocean stations. The small particles dominated by numbers everywhere. Typical particle abundances were 60–80% small particles, 15–30% medium particles, and 4–8% large particles (data not shown), indicating a consistent relative particle size distribution.

Maximum total particle volumes were 11–18 ppm at the coastal stations and 3–8 ppm at the open ocean stations (Fig. 3B). There was no subsurface particle increase in total particle volume. Despite the numerical dominance of small particles, they did not contribute much to the total particle volume. The deep ocean peak in small and medium sized particle abundance at Station 3 (Fig. 3A) was mirrored in the particle volume profile (Fig. 3B). Particles $>500\ \mu m$ contributed more than 70% to the total volume at all stations and depths (Fig. 3C). Largest marine snow particles (>1 mm) formed ~50% of the total particle volume at the coastal stations and ~20–30% at the open ocean stations (Fig. 3C). Thus, small particles were numerically dominant, while large particles were dominant by particle volume.

We observed no indications of water mass intrusion from the salinity and temperature profiles at the depths of the subsurface particle increase. There was a deep mixing layer between ~100 and ~1200 m depth, where the southward flowing NACW meets the less saline nutrient rich SACW (Fig. 2), proving the source water for surface upwelling (Hughes and Barton, 1974). There was an increase in salinity and temperature in surface waters with increasing distance from the coast, which reflected the decreased influence of the upwelling of the colder and less saline SACW away from the coast (Fig. 2).

The particle size spectra and particle volume spectra showed a general decrease in particle abundance and an increase in volume with increasing size at all stations, the spectra are only showed for Station 1 (Fig. 4A, B). The number spectra peaked at an aggregate size of ~0.2 mm for all stations. This may be caused by undercounting of smaller particles by the camera system (Fig. 4A; Jackson et al., 1997). The number spectra followed a power law distribution for particles larger than ~0.2 mm, with values of b from 1.9 to 3.4 (Fig. 4D). The steeper slopes indicate dominance of smaller particles. We observed no consistent changes in number spectra, although Stations 1 and 4 had slightly steeper slopes below 200 m depth, indicating larger dominance of small particles at these depths (Fig. 4D). Stations 1 and 3 had larger values of b slopes. The average ESD for all stations ranged from 0.37 to 0.53 mm (Fig. 4C). The largest

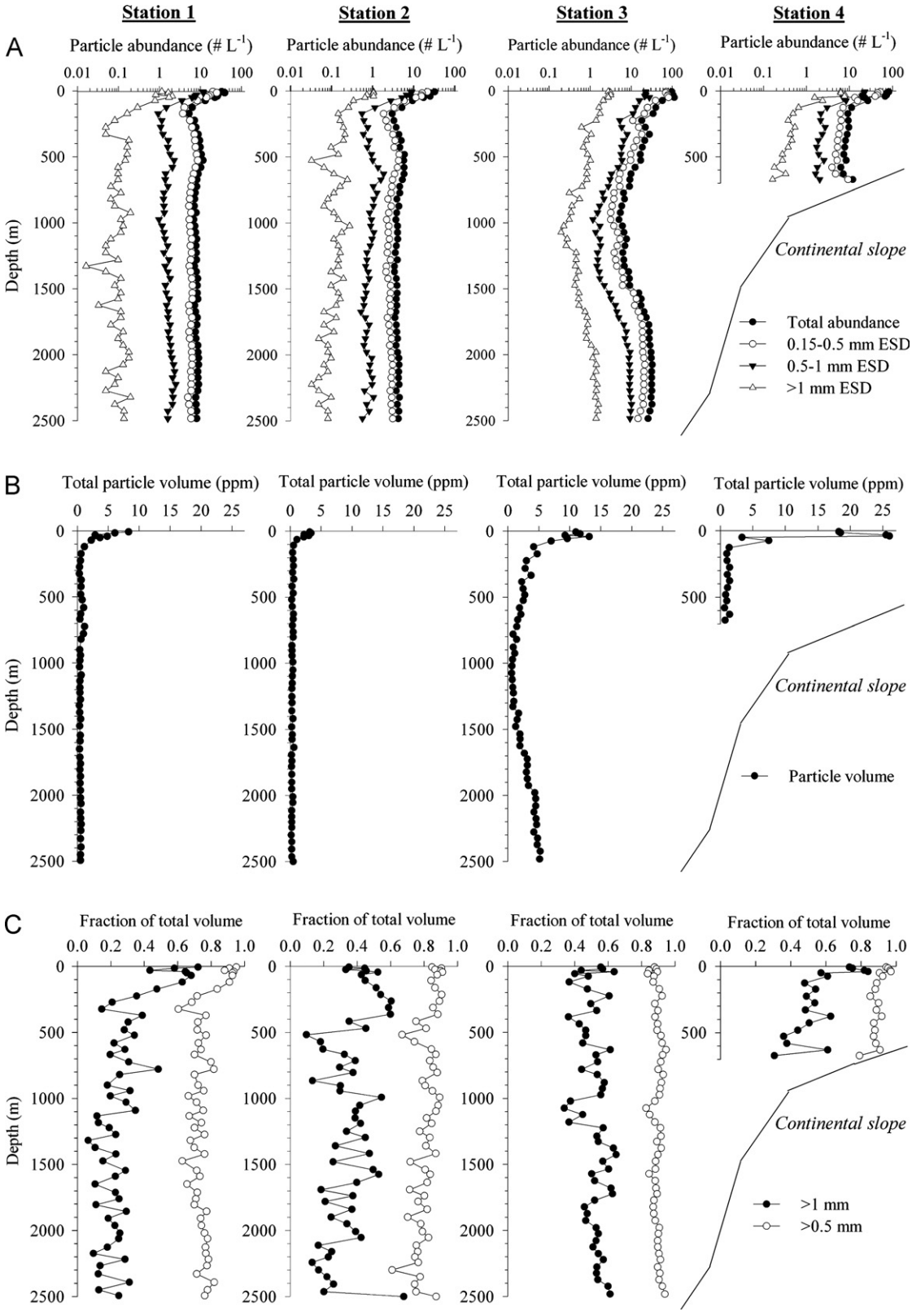

Fig. 3. *ParCa measurements.* (A) Vertical distribution of particle abundance for total particles and difference size groups of the particles recorded in the camera profiles. (B) Vertical distribution of total volume (cm^3 per m^3, ppm) of the particles measured from the camera profiles. (C) Vertical distribution of percent of total volume made up by particles larger than 0.5 mm (open circles) and larger than 1 mm (closed circles) against depth. The vertical distributions were calculated as average for 50 m bins below the upper 50 m depth.

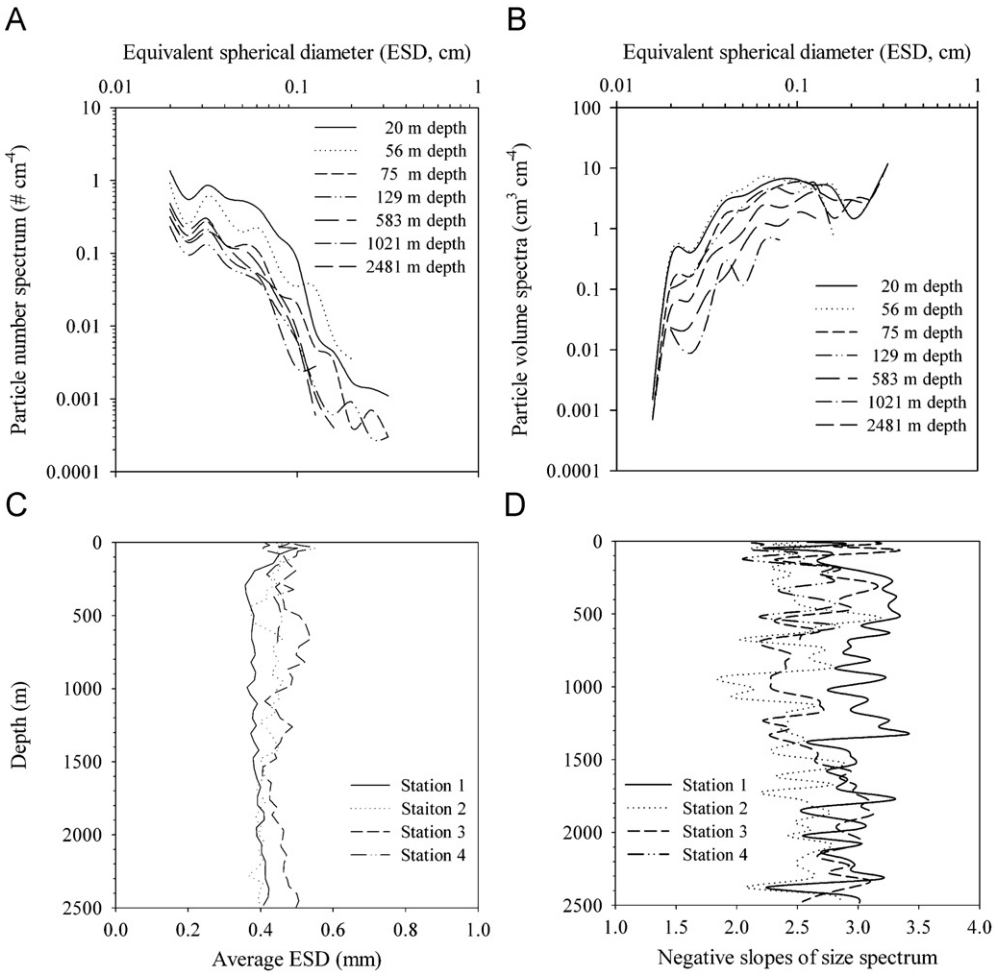

Fig. 4. *Particle size spectra and average sizes of in situ particles*. (A) Observed mean particle number size spectra (n) plotted against aggregate equivalent spherical diameter (ESD, cm) for Station 1 at different depths (see Section 2.2). The particle number size spectrum is calculated as average for 50 m bins below the upper 50 m depth. (B) Average particle volume spectra ($cm^3\ L^{-1}\ ESD^{-1}$) against equivalent spherical diameter (ESD, cm) for different depths at Station 1. (C) Average equivalent spherical diameter (ESD) for the particles observed at each depth and station. (D) Negative slopes of the particle size spectra calculated against depth for each station (see Section 2.2).

particles observed in the surface water (<150 m) was between 3.5 and 5.1 mm at all stations. At Stations 1–3 there were between 1 and 3 particles L^{-1} larger than 1 mm and fewer than 8 particles L^{-1}at Station 4.

3.3. Comparing estimated flux to sediment trap flux

We found that our regionally based data set provided a better fit to both mass and carbon fluxes from sediment traps (Table 2) than the relationship by Guidi et al. (2008b) (Fig. 5; Table 3). The estimates using the global relationship from Guidi et al. (2008b) underestimated our sediment trap fluxes by a factor of 10. The relationships from the regional relationship provided flux estimates approximately at a 1:1 ratio between estimated and measured mass and carbon fluxes at >1000 m depth (Fig. 5C and D).

3.4. Vertical profiles of spectrum-derived mass and carbon fluxes

The mass flux estimated using Eqs. (1) and (2) and our estimates for A and B value off Cape Blanc was high in the upper 150 m at all stations (Fig. 6A). The vertical mass fluxes decreased below 150 m and were relatively constant, with flux decreasing further only slowly with increasing depth. However, Station 3 had increasing mass fluxes below 1500 m (Fig. 6A).

3.5. Aggregation potential

Formation of aggregates larger than $\sim$0.5 mm equivalent spherical diameter (ESD) was observed after 2.5 h of incubation of water sampled in the fluorescence maximum in the roller tanks. The size and abundances of aggregates increased during the incubation period, reaching 1.9 ± 1.2 agg. L^{-1} after 19 h. The average ESD was 2.60 ± 1.18 mm, and ranged between 0.76 and 5.26 mm. However, in a few of the incubations the aggregated material had formed one large aggregate of a few cm, which broke into smaller aggregates when the roller tank was removed from the roller table. Because the aggregates were non-spherical, with the average ratio of longest to shortest axis $=5.7\pm4.9$, we treated them as ellipsoids when estimating their volumes and surface areas for the respiration calculations. We observed no significant differences in aggregate ESDs ($p=0.87$, one-way ANOVA), dry weights ($p=0.74$, one-way ANOVA), or settling velocities ($p=0.09$, one-way ANOVA) among the four stations and have therefore pooled data from all aggregates in subsequent analyses.

The aggregated material was dominated by diatom-derived material, especially from *Chaetoceros* sp., but also from *Thallassiosira* sp., *Nitzschia* sp., and pennate diatoms. However, the opal shells of *Chaetoceros* sp. were often broken and appeared empty, and were mainly recognizable from their spines. Coccolithophores were abundant in the aggregated material, but at lower

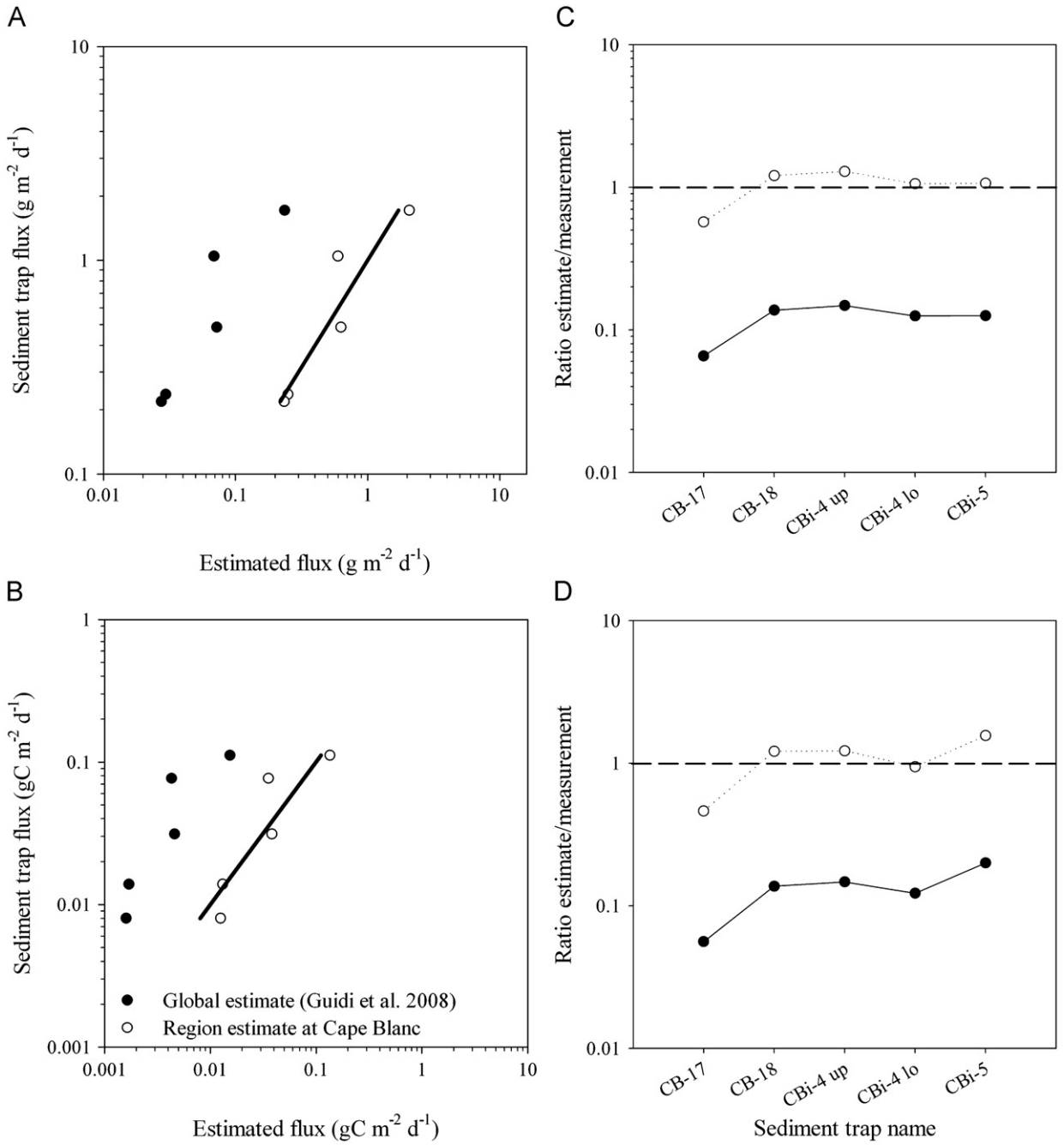

Fig. 5. *Comparison of mass fluxes*. A and B show the deep ocean sediment trap fluxes of total mass and organic carbon plotted against the estimated flux using Eqs. (1) and (2) for both local (open circles) and global (closed circles) flux estimates. The solid lines show the 1:1 ratio. C and D show the ratio of estimated flux to sediment trap fluxes for both local (open circles) and global (closed circles) flux estimates. The dashed line indicates the 1:1 ratio.

abundances than diatoms. *Emiliania huxley* was the dominant coccolithophore in the aggregated material. *Chaetoceros* sp. was 2×10^4–30×10^4 higher in numerical abundance than *E. huxley*. Liths of *E. huxley* were 10–10^6 times more abundant in the aggregates than whole coccolithophorids (Table 4). Other material in aggregates included empty frustules, setae, copepod fecal pellets, clay minerals, small grains of quartz, and unidentified lithogenic material. The aggregates formed in the rolling tanks appeared highly porous (Fig. 7A and B). The relative aggregation potential of the suspended material in the water was estimated as the fraction of initial material found in the water sample (Table 4).

The dry weight increased with increasing aggregate diameter, from 2.55 to 451 μg per aggregate. One aggregate had more than twice the dry weight (856 μg) than similar sized aggregates (~5.2 mm ESD) and was excluded from the data analyses (Fig. 8A). The POC content in the aggregated material ranged between 1.8 and 591 μgC agg.$^{-1}$, and also increased with aggregate diameter. The aggregates had an inorganic carbon to dry weight ratio of 0.075 ± 0.014, and a $CaCO_3$ to POC ratio of 0.09. Particulate content of the source water was 254 ± 163 μgC L^{-1} and had C:N$= 5.3 \pm 0.36$. Table 5 shows the POC:DW for suspended particles at the depths of fluorescence maximum, from material collected by deep ocean sediment traps, and from the aggregates formed during the roller tank incubations.

Settling velocity increased with increasing aggregate sizes, and ranged from 88 to 569 m d^{-1} (Fig. 8B). The respiration rate per

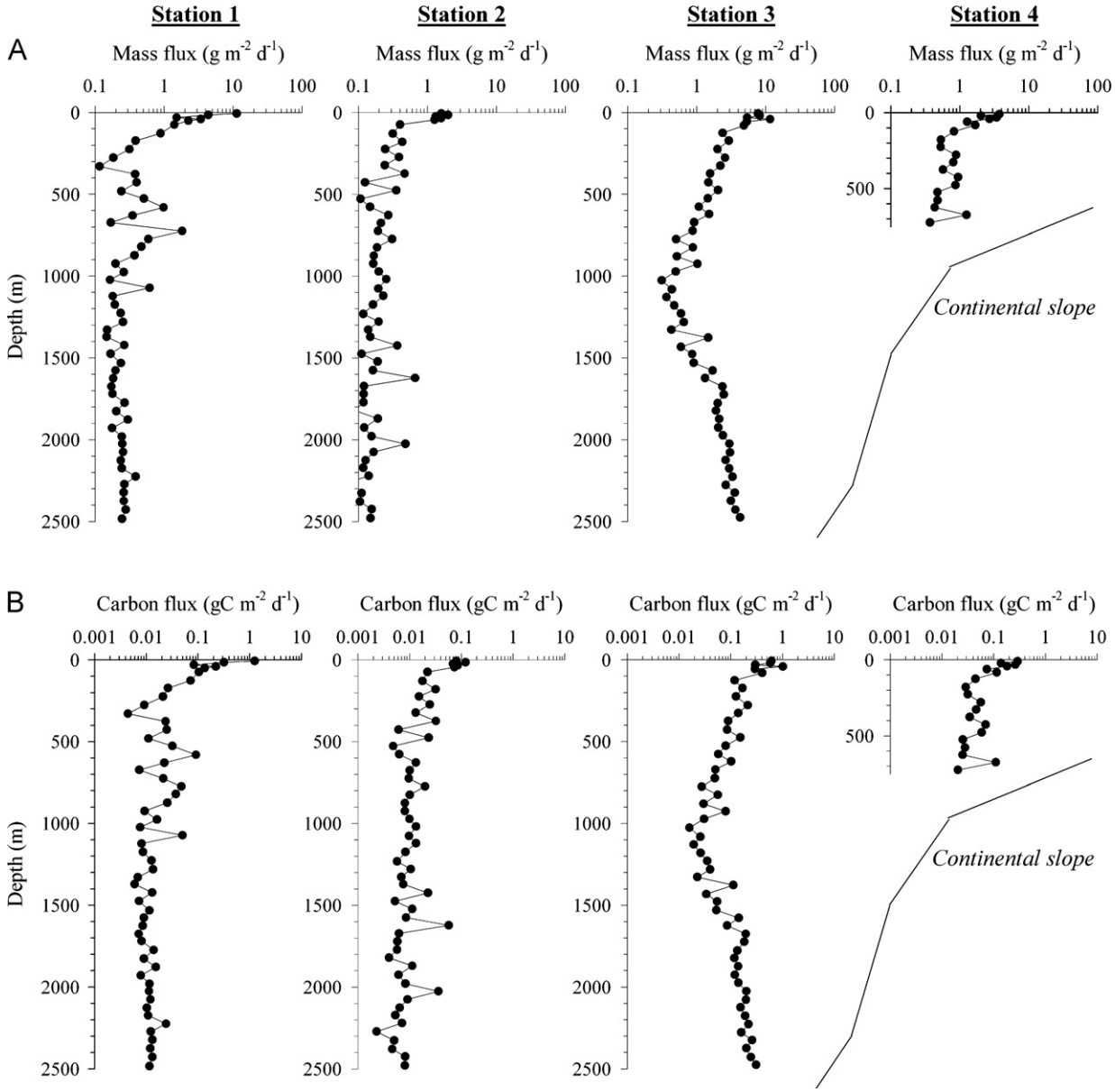

Fig. 6. *Estmated mass and carbon fluxes*. Aggregated (A) mass fluxes (g m^{-2} d^{-1}) and (B) organic carbon fluxes (gC m^{-2} d^{-1}) estimated from Eqs. (1) and (2) using the local relationship of *A* and *B* related to sediment trap fluxes and vertical particle size distributions. Measurements for the coastal station were made only to a depth of 700 m due to shallower water depth.

aggregate also increased with increasing aggregate size, and it ranged from 19.0 to 729 ngC h^{-1} (Fig. 8C). One ~5 mm aggregate had a very high respiration rate (1.66 μgC h^{-1}) and was excluded from the analysis. The respiration rate was proportional to aggregate POC content (data not shown). Hence, the fractional remineralization rate during exponential decay with time (*R*) was 0.13 ± 0.07 d^{-1}, and independent of aggregate size (Fig. 8D). The fractional remineralization per meter settled (*R*: sinking velocity) is referred to as the remineralization length scale, *L* (m^{-1}), providing a different water column perspective of the remineralization. *L* ranged between 0.05 and 3.23 km^{-1} and decreased with increasing aggregate size (Fig. 8E).

3.6. Flux derived ratio of L (L_{fl})

A flux-derived *L* (m^{-1}) can be estimated separately from the flux data by assuming a constant fraction is being degraded per depth interval; $dF/dz = -Lz$. This has the solution; $F = F_0\, exp^{-Lz}$. Thus, the flux derived *L* can be found via $L_{fl} = -\ln(F_z/F_{z0})/(z - z_0)$. We estimated L_{fl} for the depth intervals 40–150 and 150–250 m, and plotted this together with *L* from the roller tank formed aggregates (Fig. 9). The solid and dashed lines show the standardized $L \pm SD$ at constant *R* divided by the estimated sinking velocity ($w = R/a\ ESD^b$). L_{fl} is higher than *L* for both the upper (40–150 m) and the lower (150–250) depth intervals. However, L_{fl} was closer to *L* for the smaller relative to the larger particle sizes, resulting in L_{fl} having constant loss per depth across the particle size spectrum (Fig. 9).

4. Discussion

The *in situ* particle numerical abundances were well within the range of marine snow concentrations found in previous studies, but the total volumes were in the lower end (< 17 ppm) of

Table 4
Aggregation potential shown as the ratio of material aggregated during roller tanks incubations (agg.) to the concentration of suspended material (susp. mat.) in the water samples before incubation.

Aggregated material	Ratio of agg.: susp. mat.	Concentration of susp. mat.
Emiliania huxley, coccoliths	0.44 ± 0.33	$53.9 \pm 30 \times 10^5$ L^{-1}
Emiliania huxley, whole	0.33 ± 0.58	$2.4 \pm 1.9 \times 10^5$ L^{-1}
Prymnesiophyta, coccoliths	0.33 ± 0.58	$1.6 \pm 1.4 \times 10^5$ L^{-1}
Prymnesiophyta, whole	0	$0.2 \pm 0.1 \times 10^5$ L^{-1}
Chaetoceros sp., spines	0.07 ± 0.1	$52.1 \pm 10.3 \times 10^5$ L^{-1}
Thallasiosira sp.	0.18 ± 0.32	$1.2 \pm 1.6 \times 10^5$ L^{-1}
Pennate diatoms	0	$2.2 \pm 3.1 \times 10^5$ L^{-1}
Dry weight	0.18	2.1 ± 0.6 mg L^{-1}
Particulate organic carbon	0.5	0.3 ± 0.2 mgC L^{-1}

Water samples were collected at the depth of fluorescence maximum. The aggregation potential is illustrated as the ratio of total aggregated dry weight and particulate organic carbon (POC) to the dry weight and POC of suspended particles in the water samples before incubation.

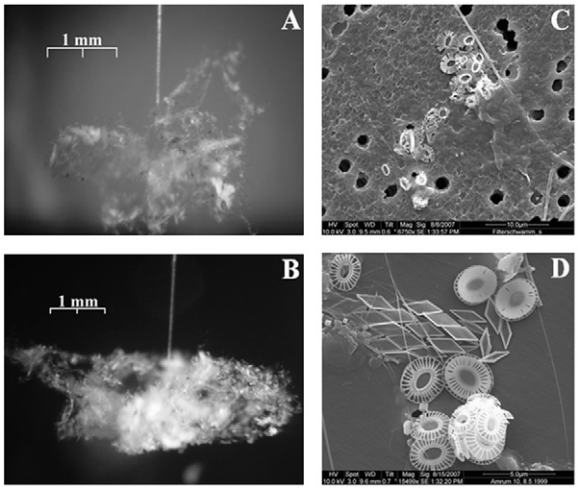

Fig. 7. *Pictures of aggregates and their constitutes.* (A) Three-mm large aggregate seen from above during suspension. (B) Three-mm large aggregate seen from the side during suspension. (C) Scanning electron microscopic picture of coccoliths from *Emiliania huxleyi* found within an aggregate. (D) Scanning electron microscopic picture of coccoliths from *Emaliana huxley* collected from a seawater sample.

previous observations (Fig. 3B; e.g. Graham et al., 2000; Lampitt et al., 1993; MacIntyre et al., 1995). Hence, the particle spectrum off Cape Blanc was more dominated by smaller particles as compared with other sites. This pattern was observed during an earlier 3-year study off Cape Blanc (Nowald et al., 2006), and seems to be a general property of the particle size distributions there. Laboratory studies have shown that incorporation of lithogenic matter into aggregates can result in the formation of small aggregates (Hamm, 2002). In addition, scavenging of lithogenic matter by large aggregates causes them to fragment into smaller particles (Passow and De La Rocha, 2006). The area off Cape Blanc has high concentrations of lithogenic matter due to the enhanced dust input from the atmosphere. Indications of fragmentation were observed from the slight decrease in average particle size and change in particle size spectrum between ~100 and 300 m depth (Fig. 4C and D). Below 300 m depth the abundance and size distribution of particles did not show any significant changes with increasing depth (Figs. 3A and 4C, D), indicating the <300 m as the active aggregation/disaggregation zone. Incorporation of lithogenic matter into biogenic particles in the upper ocean may increase their specific weight and potentially increase their sinking velocity, leading to increased particle transport to depth >300 m where aggregation is slow or absent. Thus, the dominance of small particles could result from lithogenically induced breakup and higher settling rates out of surface waters for smaller particles. Zooplankton activity might also be an important fragmentation process (Dilling and Alldredge, 2000; Iversen and Poulsen, 2007; Kiørboe, 2000), but was not investigated during our study.

Highest particle abundances were observed in the surface waters, and it decreased rapid with depth within the upper 150 m (Fig. 3A and B). Fluorescence maxima were measured within the depth of the surface particle maxima (Table 1), indicating that those particles might contain high amounts of phytoplankton material. The particle abundance in the surface maxima decreased with increasing distance from the coast (Fig. 3A), which is consistent with higher primary production near the coast resulting from upwelling (Fig. 2). Thus, the particle abundance in the surface waters seemed closely linked to the biomass of primary producers and may contain a large fraction of phytoplankton. This is supported by the high aggregation potential of particles in the fluorescence maximum and the high POC:DW ratio of aggregates in our study as well as by a numerical experiment where the surface particle maximum off Cape Blanc could be explained by local biological productivity (Karakas et al., 2006).

Increases in particle abundance were found in the subsurface layers at ~300 and ~500 m depths for the coastal and open ocean sites, respectively (Fig. 3A). We observed very low fluorescence within the subsurface particle maxima (data not shown), indicating small contributions from phytoplankton there. This is consistent with the results of Karakas et al. (2006), who found no connections between the surface particle maxima and subsurface number increase off Cape Blanc and argued that the increases in abundance in the subsurface were not explained by biological activity alone. Using numerical modelling, Karakas et al. (2006) were able to reproduce previous observed subsurface particle numbers off Cape Blanc (Nowald et al., 2006) by "releasing" particles on the shallow shelf area off Cape Blanc and allowing them to be transported offshore with an average settling velocity of 5 m d^{-1}. They suggested that the subsurface particle increase originated from offshore transport of eroded or resuspended material from the shallow shelf. The particle abundance profiles (Fig. 3A) showed increasing particle abundance in the surface dominated by particles in the size range 150–500 μm. Thus, the particle sizes making up the subsurface increase had little influence on the total particle volume profiles (Fig. 3B). Still, the subsurface abundance increase might influence the particles settling through these depths by incorporation of eroded or resuspended inorganic particles with high specific densities, leading to increased aggregate densities, as suggested by Fischer et al. (2009b).

Both this and previous studies (Karakas et al., 2006; Nowald et al., 2006) have observed a rapid vertical decrease in particle abundance and total volume within the upper 150 m of the water column off Cape Blanc (Fig. 3A and B). Low fluorescence within the subsurface increase in particle abundance, lack of connections between the particles in the surface maxima, and increase in subsurface abundance (Karakas et al., 2006), indicate the vertical decrease in total particle abundance and volume at <150 m might be due to rapid degradation and/or remineralisation of the organic material within the settling particles. Thus, the particles found at the surface presumably differ from the particles at greater depth. We expect them to be more porous and less dense due to their higher content of organic matter, as observed for the particles formed during incubation of surface water. Therefore the particles formed during the incubations are only representative for the particles observed in the surface waters (<150 m depth) off Cape Blanc.

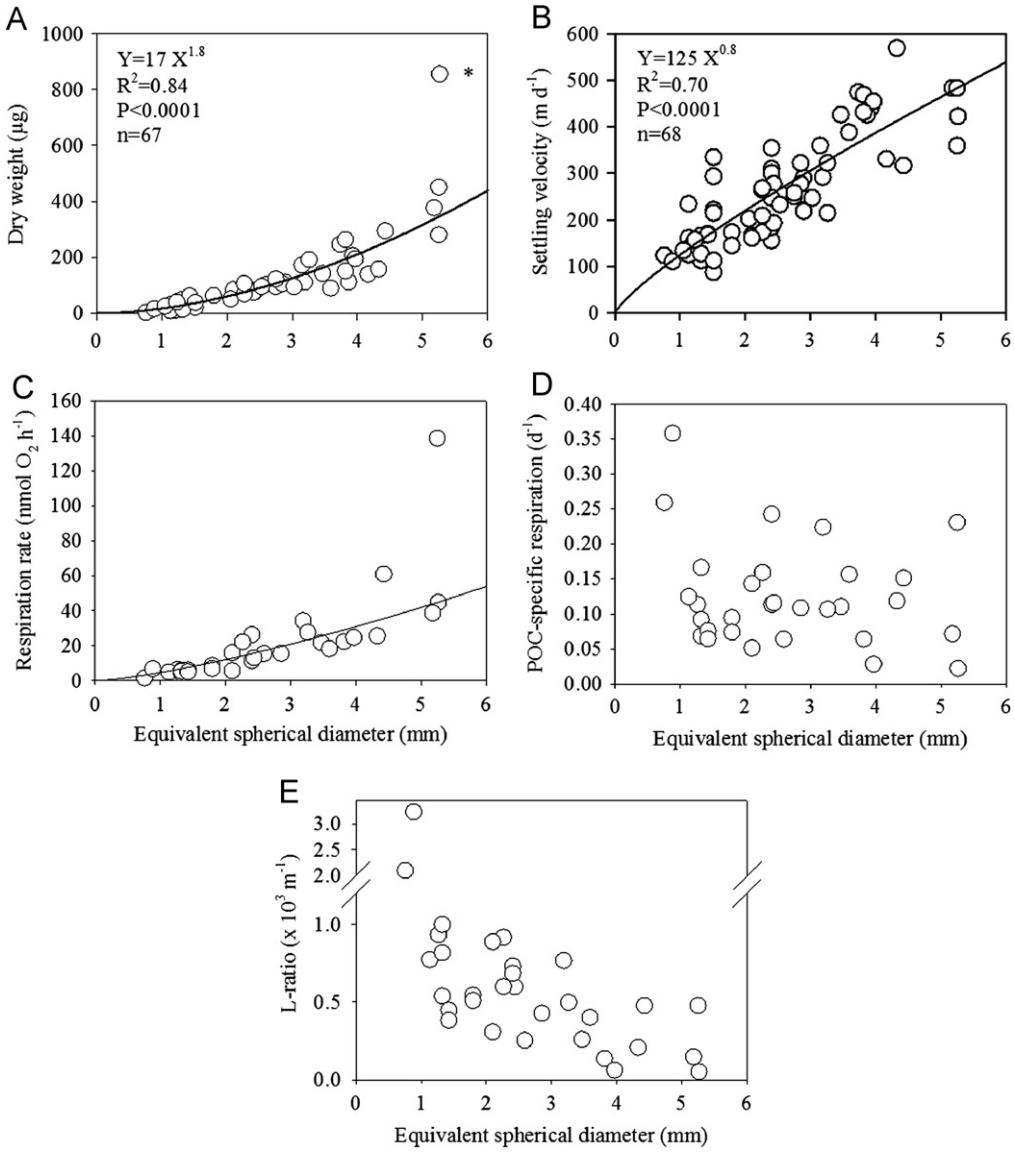

Fig. 8. *Size-specific measurements of marine snow aggregates.* (A) Aggregate dry weight as a function of diameter. The solid line represents a power fit to the measurements. The ∗ indicates that the aggregate is excluded from the regression. (B) Aggregate settling velocity as a function of size. The solid line represents a power fit to the measurements. (C) Measured respiration rate as a function of aggregate size. The solid line represents a power fit to the measurements. The ∗ indicates that the aggregate is excluded from the regression. (D) POC-specific respiration rate as a function of aggregate diameter. (E) *L* ratio as a function of aggregate size.

Table 5
Ratios of particulate organic carbon (POC) to dry weight (DW).

Types of measured particles	POC:DW
Agg. potential incubations	0.39 ± 0.02
Suspended particles collected at fluorescence maximum	0.12 ± 0.05
Material collected with deep ocean sediment traps	0.06 ± 0.01

Three types of particles were used to estimate the POC:DW ratios; aggregates formed from incubations of material collected at fluorescence maximum (Agg. potential incubation), suspended particles from water samples collected at fluorescence maximum and retrained on GF/F filters, and material collected using deep ocean sediment traps.

Organic matter in the surface waters showed a high aggregation potential (Table 4), and a large fraction of the composite material within the aggregates formed from surface material was of biogenic origin (Table 5). However, due to sampling limitations no direct measurements could be made on *in situ* formed aggregates. The aggregates formed during our incubation experiments indicated diatoms as the most important phytoplankton in aggregate formation (Table 4) as also observed in previous studies (Alldredge and Silver, 1988). Furthermore, our data suggest that coccoliths were scavenged by the aggregates when settling through the water column. Scavenging by aggregates has been suggested previously as a mechanism enhancing downward transport of coccoliths (see De La Rocha and Passow, 2007). We also observed the presence of inorganic lithogenic material within the aggregates which, together with carbonates, may ballast the aggregates and lead to increased fluxes (Armstrong et al., 2002; Francois et al., 2002; Klaas and Archer, 2002). Previous flux measurements using deep ocean sediment traps have shown incorporation of carbonate and lithogenic material in sedimenting material off Cape Blanc (Fischer et al., 2009a). We suggest that high diatom concentrations are important precursors for aggregate formation and that high atmospheric dust input together with high carbonate production lead to increased fluxes off Cape Blanc via ballasting.

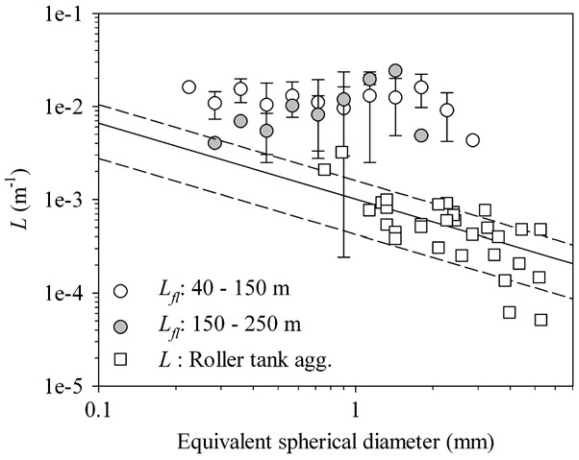

Fig. 9. *Flux-derived ratio of L. Shows L* derived from the estimated carbon flux profiles between 40 and 150 m (open circles), between 150 and 250 m (grey circles), and *L* for aggregates formed during incubation of water collected at fluorescence maximum (open squares) plotted against the aggregate size (ESD, mm). The solid line indicates the theoretical *L* at constant *R* divided by power-law w ($=R/a$ ESD^b), and the dashed lines indicate *L* calculated for $R \pm$ SD.

Total fluxes measured using sediment traps represent the sum of fluxes for particles with a wide range of sizes and settling velocities. This summation over particle types loses information about spatial coverage and the particle size distribution, resulting in loss of the ability to make mechanistic descriptions of particle dynamics. By relating the aggregate size distribution obtained by vertical camera profiles with deep ocean fluxes from traps, particle fluxes can be estimated at greater vertical and horizontal resolutions (Guidi et al., 2008b). However, this method is limited by the accuracy of the relationships used to convert among particle diameter, particle mass, and settling speed (Eqs. (1) and (2)). Thus, using one relationship throughout the water column precludes changes in size-specific sinking velocity with depth (e.g. Berelson, 2002; Fischer and Karakas, 2009) and changes in carbon to dry weight with depth when making high resolution estimates of vertical fluxes.

The consistent underestimation of fluxes when using the values of Guidi et al. (2008b) might be due to biogeochemical differences in the oceanic regions. Our study site at the continental margin off NW Africa is an upwelling system with high productivity (Carr, 2002), while the data used by Guidi et al. (2008b) were measured at open ocean sites in the Pacific, North Atlantic, and Mediterranean Sea. The oceanic regions used by Guidi et al. (2008b) all have lower fluxes of organic carbon and carbonate (Honjo et al., 2008) than those measured off Cape Blanc in this and previous studies (Fischer et al., 2009b). Therefore, the size-specific mass and sinking velocity of the particles off Cape Blanc appear not to be comparable with the size-specific particle properties in the regions investigated by Guidi et al. (2008b), leading to underestimations in inferred organic carbon and mass fluxes. Thus, it seems important to know the composition of particles of the study area before choosing the *A* and *B* values used to estimate fluxes from relations of particle size distribution and sediment trap fluxes. This importance has been demonstrated by Ploug et al. (2008), who found that sinking velocities of different particle types depend on source, density, and age of the particles rather on their size alone.

Our observation that the largest decrease in carbon fluxes was in the upper ~150 m of the water column is consistent with results from previous studies reporting quasi-exponential declines in flux with increasing depth (e.g. Martin et al., 1987; Schlitzer, 2000; Suess, 1980), indicating that most of the POC is decomposed in the surface ocean. The degradation of organic carbon has been suggested as carried out by zooplankton and microbes (see De La Rocha and Passow, 2007 and references therein). In the present study we found that the average microbial carbon-specific carbon respiration rate was relatively constant for all aggregate sizes. This has also been observed in diatom aggregates collected off the coastal California (Ploug et al., 1999) and in aggregates formed on diatom detritus (Ploug and Grossart, 2000). The carbon-specific respiration rates in our ballasted aggregates were similar to those measured on non-ballasted diatom aggregates by Ploug et al. (1999). Hence, we did not observe any evidence that incorporation of carbonate and/or lithogenic material provide protection from bacterial remineralization of labile organic carbon, as also suggested by other studies (Ploug et al., 2008).

Since all surface aggregates seem remineralized at similar carbon-specific rates, the extent of their remineralization in the upper water column is determined by their residence times, indicating sinking velocity as a controlling factor for organic carbon export. This is consistent with the remineralization length scale, *L*, derived from the roller tank formed aggregates, which decreases with increasing aggregate size due to the faster sinking speed of large aggregates relative to smaller ones (Fig. 8E). However, *L* from the roller tank formed aggregates is calculated assuming microbial respiration to be the sole carbon sink on aggregates. Hence, the higher L_{fl} values derived from *in situ* particle spectra and fluxes presumably result from additional processes than just microbial respiration contributing to the degradation of aggregates (Fig. 9), such as ecto-enzymatic hydrolysis (Smith et al., 1992), grazing by zooplankton (Dilling and Alldredge, 2000), and aggregate fragmentation induced by incorporation of lithogenic matter (Hamm, 2002; Passow and De La Rocha, 2006) and/or zooplankton fragmentation (e.g. Iversen and Poulsen, 2007). The constant degradation length scale across the particle size spectrum, L_{fl}, indicates flux feeding as the dominant mode of particle loss (Fig. 9), since flux feeding caused a decrease in flux proportional to particle sinking speed and concentration (Jackson, 1993). Hence, the decrease in *L* with increasing particle is counter-acted by preferential flux feeding on large fast-sinking particles. Filter feeding is not indicated as an important mechanism for the particle loss, since filter feeding decreases with increasing particle size (e.g. Iversen and Poulsen, 2007; Poulsen and Kiørboe, 2005) and would be observed as a decrease in L_{fl} with increasing particle size. We therefore suggest zooplankton flux feeding as an important carbon removal process in the upper water column during our study period off Cape Blanc. This is consistent with previous findings indicating zooplankton (e.g. Dilling and Alldredge, 2000; Kiørboe, 2000; Steinberg, 1995) and protozooplankton (Poulsen and Iversen, 2008) degradation processes important for carbon removal in the upper water column. However, microbial degradation might be dominant at deeper depths as zooplankton becomes rare at these depths.

Previous studies have suggested that sinking speeds measured in laboratories are the potential maximum sinking speeds, and that aggregates *in situ* will experience much longer residence times in the upper ocean than predicted from such measurements (Alldredge and Gotschalk, 1988). However, if degradation and remineralization of aggregates are only due to aggregate-attached bacteria, the average sinking velocity, *w*, estimated from L_{fl} should be 11.5 ± 5.5 m d^{-1} (data not shown), which is 3-fold lower than the average *in situ* sinking velocity for 0.5 mm large non-ballasted diatom aggregates (Alldredge and Gotschalk, 1988). Further, L_{fl} was constant across the particle size spectrum, indicating that sinking velocity should be constant across all particle sizes. The roller tank aggregates showed clear size dependency in sinking velocity, and does, therefore, not support a constant sinking

velocity for *in situ* particles. Thus, zooplankton flux feeding may be an additional important degradation process for the carbon removal in the upper ocean.

It has been shown that attached bacteria may have markedly higher cell-specific hydrolytic enzyme activity relative to the free-living bacteria. The coupling between hydrolysis and subsequent assimilation and respiration by attached bacteria may at times be inefficient, leading to a release of dissolved organic carbon (DOC) to the bulk water. The released DOC is partly assimilated and partly respired by free-living microbes (Cho and Azam, 1988; Kiørboe and Jackson, 2001; Smith et al., 1992). The leakage of DOC from the settling aggregates creates a plume in their wake (Kiørboe and Jackson, 2001). This plume potentially helps horizontal cruising zooplankton organisms in their detection and encounter of aggregates via chemical perception (Kiørboe and Thygesen, 2001), which would increase flux feeding. Flux feeding is supported by observations of pelagic copepods with adaptations to feed on solid surfaces, such as aggregates (Kiørboe, 2001), and by previous studies that suggested carbon removal via zooplankton activity (Banse, 1990) and direct feeding on marine aggregate by copepods (Green and Dagg, 1997; Koski et al., 2005; Steinberg et al., 1994). We therefore suggest flux feeding organisms are important in controlling carbon recycling, as also suggested by Jackson (1993).

The constant carbon fluxes at mid-water depths and to the deep ocean relative to surface fluxes indicate little decomposition of organic carbon at these depths (Fig. 6B). This is supported by previous studies that found the cycling of organic carbon in the deep ocean at rates orders of magnitudes lower than in the surface waters (Nagata et al., 2000; Reinthaler et al., 2006). The constant fluxes may indicate that the bacterial activity is limited in the deep ocean, i.e. due to low amounts of labile organic matter in the aggregates, low *in situ* temperatures, decreased bacterial abundance (e.g. Nagata et al., 2000) and/or activity (Morita, 1984) with depth, changes in bacterial community with depth, detachment of bacteria (Kiørboe, 2003; Kiørboe et al., 2003), etc. However, any conclusive explanation to the low degradation rates at depth cannot be made without further studies of deep ocean aggregate processes. Still, microbes seem to be the main degraders influencing the carbon fluxes in the deep ocean and the deep mid-water zones as zooplankton are rare at these depths, as also suggested by Stemmann et al. (2004a).

Acknowledgments

We thank Klaus-Uwe Richter and Christiane Lorenzen for assistance during POC measurements. The oxygen microelectrodes were constructed by Gaby Eickert, Ines Schröder, and Karin Hohmann, Max Planck Institute for Marine Microbiology, Bremen. We thank the captain and crew on the research vessel Maria S. Merian cruise leg MSM04/4b, March/April 2007. We also thank Uta Passow and Thomas Kiørboe for useful discussions. We thank Philip Boyd and two anonymous reviewers for their thoughtful comments, which improved the manuscript.

This study was supported by the Helmholtz Association (to H.P.) and the Alfred Wegener Institute for Polar and Marine Research (to M.H.I. and H.P.). This is AWI publication no. awi-n 18537. This study was funded through the DFG-Research Center/Cluster of Excellence "The Ocean in the Earth System" (to M.H.I., N.N., G.F., and H.P.).

References

Alldredge, A., Gotschalk, C., 1988. *In situ* settling behavior of marine snow. Limnol. Oceanogr. 33 (3), 339–351.

Alldredge, A.L., Silver, M.W., 1988. Characteristics, dynamics and significance of marine snow. Prog. Oceanogr. 20 (1), 41–82.

Armstrong, R.A., Lee, C., Hedges, J.I., Honjo, S., Wakeham, S.G., 2002. A new, mechanistic model for organic carbon fluxes in the ocean based on the quantitative association of POC with ballast minerals. Deep-Sea Res. II 49 (1–3), 219–236.

Asper, V.L., 1987. Measuring the flux and sinking speed of marine snow aggregates. Deep-Sea Res. 34, 1–17.

Banse, K., 1990. New views on the degradation and disposition of organic particles as collected by sediment traps in the open sea. Deep-Sea Res. 37, 1177–1195.

Berelson, W.M., 2002. Particle settling rates increase with depth on the ocean. Deep-Sea Res. II 49, 237–251.

Bory, A.J.M., Newton, P.P., 2000. Transport of airborne lithogenic material down through the water column in two contrasting regions of the eastern subtropical North Atlantic Ocean. Global Biogeochem. Cycles 14 (1), 297–315.

Boyd, P.W., Trull, T.W., 2007. Understanding the export of biogenic particles in oceanic waters: is there consensus? Prog. Oceanogr. 72 (4) 276–312.

Buesseler, K.O., Antia, A.N., Chen, M., Fowler, S.W., Gardner, W.D., Gustafsson, O., Harada, K., Michaels, A.F., van der Loeff'o, M.R., Sarin, M., Steinberg, D.K., Trull, T., 2007a. An assessment of the use of sediment traps for estimating upper ocean particle fluxes. J. Mar. Res. 65 (3), 345–416.

Buesseler, K.O., Lamborg, C.H., Boyd, P.W., Lam, P.J., Trull, T.W., Bidigare, R.R., Bishop, J.K.B., Casciotti, K.L., Dehairs, F., Elskens, M., Honda, M., Karl, D.M., Siegel, D.A., Silver, M.W., Steinberg, D.K., Valdes, J., Van Mooy, B., Wilson, S., 2007b. Revisiting carbon flux through the ocean's twilight zone. Science 316 (5824), 567–570.

Carr, M.E., 2002. Estimations of potential productivity in Eastern Boundary Currents using remote sensing. Deep-Sea Res. II 49, 59–80.

Cho, B.C., Azam, F., 1988. Major role of bacteria in biogeochemical fluxes in the ocean's interior. Nature 332 (6163), 441–443.

De La Rocha, C.L., Passow, U., 2007. Factors influencing the sinking of POC and the efficiency of the biological carbon pump. Deep-Sea Res. II 54 (5–7), 639–658.

Dilling, L., Alldredge, A.L., 2000. Fragmentation of marine snow by swimming macrozooplankton: a new process impacting carbon cycling in the sea. Deep-Sea Res. I 47, 1227–1245.

Fischer, G., Karakas, G., 2009. Sinking rates and ballast composition of particles in the Atlantic Ocean: implications for the organic carbon fluxes to the deep ocean. Biogeosciences 6, 85–102.

Fischer, G., Karakas, G., Blaas, M., Ratmeyer, V., Nowald, N., Schlitzer, R., Helmke, P., Davenport, R., Donner, B., Neuer, S., Wefer, G., 2009a. Mineral ballast and particle settling rates in the coastal upwelling system off NW Africa and the South Atlantic. Int. J. Earth Sci. 98, 281–298.

Fischer, G., Reuter, C., Karakas, G., Nowald, N., Wefer, G., 2009b. Offshore advection of particles within the Cape Blanc filament, Mauritania: results from observational and modelling studies. Prog. Oceanogr. 83, 322–330.

Fischer, G., Wefer, G., 1991. Sampling, preparation and analysis of marine particulate matter. In: Hurd, D.C., Spencer, D.W. (Eds.), Marine Particles: Analysis and Characterization. Geophysical Monograph, pp. 391–397.

Fowler, S.W., Knauer, G.A., 1986. The role of large particles in the transport of elements and organic compounds through the oceanic water column. Prog. Oceanogr. 16, 147–194.

Francois, R., Honjo, S., Krishfield, R., Manganini, S., 2002. Factors controlling the flux of organic carbon to the bathypelagic zone of the ocean. Global Biogeochem. Cycles 16 (4, doi:10.1029/2001GB001722.

Gorsky, G., Aldorf, C., Kage, M., Picheral, M., Garcia, Y., Favole, J., 1992. Vertical distribution of suspended aggregates determined by a new underwater video profiler. Ann. Inst. Océanogr. 68, 275–280.

Graham, W.M., MacIntyre, S., Alldredge, A.L., 2000. Diel variations of marine snow concentration in surface waters and implications for particle flux in the sea. Deep-Sea Res. I 47 (3), 367–395.

Green, E.P., Dagg, M.J., 1997. Mesozooplankton associations with medium to large marine snow aggregates in the northern Gulf of Mexico. J. Plankton Res. 19 (4), 435–447.

Guidi, L., Gorsky, G., Claustre, H., Miquel, J.C., Picheral, M., Stemmann, L., 2008a. Distribution and fluxes of aggregates $>100\,\mu m$ in the upper kilometer of the South-Eastern Pacific. Biogeosciences 5 (5), 1361–1372.

Guidi, L., Jackson, G.A., Stemmann, L., Miquel, J.C., Picheral, M., Gorsky, G., 2008b. Relationship between particle size distribution and flux in the mesopelagic zone. Deep-Sea Res. I 55 (10), 1364–1374.

Hamm, C.E., 2002. Interactive aggregation and sedimentation of diatoms and clay-sized lithogenic material. Limnol. Oceanogr. 47 (6), 1790–1795.

Honjo, S., Manganini, S.J., Krishfield, R.A., Francois, R., 2008. Particulate organic carbon fluxes to the ocean interior and factors controlling the biological pump: a synthesis of global sediment trap programs since 1983. Prog. Oceanogr. 76 (3), 217–285.

Hughes, P., Barton, E.D., 1974. Stratification and water mass structure in the upwelling area off northwest Africa in April/May 1969. Deep-Sea Res. 21, 611–628.

Iversen, M.H., Poulsen, L.K., 2007. Coprorhexy, coprophagy, and coprochaly in the copepods *Calanus helgolandicus*, *Pseudocalanus elongatus*, and *Oithona similis*. Mar. Ecol. Prog. Ser. 350, 79–89.

Jackson, G.A., 1993. Flux feeding as a mechanism for zooplankton grazing and its implications for vertical particulate flux. Limnol. Oceanogr. 38 (6), 1328–1331.

Jackson, G.A., Maffione, R.E., Costello, D.K., Alldredge, A.L., Logan, B.E., Dam, H.G., 1997. Particle size spectra between $1\,\mu m$ and $1\,cm$ at Monterey Bay determined using multiple instruments. Deep-Sea Res. I 44, 1739–1767.

Jannasch, H.W., Zafiriou, O.C., Farrington, J.W., 1980. A sequencing sediment trap for time-series studies of fragile particles. Limnol. Oceanogr. 25 (5), 939–943.
Karakas, G., Nowald, N., Blaas, M., Marchesiello, P., Frickenhaus, S., Schlitzer, R., 2006. High-resolution modeling of sediment erosion and particle transport across the northwest African shelf. J. Geophys. Res. 111, doi:10.1029/2005JC003296.
Kiørboe, T., 2000. Colonization of marine snow aggregates by invertebrate zooplankton: abundance, scaling, and possible role. Limnol. Oceanogr. 45 (2), 479–484.
Kiørboe, T., 2001. Formation and fate of marine snow: small-scale processes with large-scale implications. Sci. Mar. 65, 57–71.
Kiørboe, T., 2003. Marine snow microbial communities: scaling of abundances with aggregate size. Aquat. Microb. Ecol. 33 (1), 67–75.
Kiørboe, T., Jackson, G.A., 2001. Marine snow, organic solute plumes, and optimal chemosensory behavior of bacteria. Limnol. Oceanogr. 46 (6), 1309–1318.
Kiørboe, T., Lundsgaard, C., Olesen, M., Hansen, J.L.S., 1994. Aggregation and sedimentation processes during a spring phytoplankton bloom: a field experiment to test coagulation theory. J. Mar. Res. 52, 297–323.
Kiørboe, T., Tang, K., Grossart, H., Ploug, H., 2003. Dynamics of microbial communities on marine snow aggregates: colonization, growth, detachment, and grazing mortality of attached bacteria. Appl. Environ. Microbiol. 69 (6), 3036–3047.
Kiørboe, T., Thygesen, U.H., 2001. Fluid motion and solute distribution around sinking aggregates. II. Implications for remote detection by colonizing zooplankters. Mar. Ecol. Prog. Ser. 211, 15–25.
Klaas, C., Archer, D.E., 2002. Association of sinking organic matter with various types of mineral ballast in the deep sea; implications for the rain ratio. Global Biogeochem. Cycles 16 (4), doi:10.1029/2001GB001765.
Koski, M., Kiørboe, T., Takahashi, K., 2005. Benthic life in the pelagic: aggregate encounter and degradation rates by pelagic harpacticoid copepods. Limnol. Oceanogr. 50 (4), 1254–1263.
Lampitt, R.S., Wishner, K.F., Turley, C.M., Angel, M.V., 1993. Marine snow studies in the Northeast Atlantic ocean: distribution, composition and role as a food source for migrating plankton. Mar. Biol. 116 (4), 689–702.
Maas, L.R.M., 1994. On the surface area of an ellipsoid and related integrals of elliptic integrals. J. Comp. Appl. Math. 51, 237–249.
MacIntyre, S., Alldredge, A.L., Gotschalk, C.C., 1995. Accumulation of marine snow at density discontinuities in the water column. Limnol. Oceanogr. 40 (3), 449–468.
Martin, J.H., Knauer, G.A., Karl, D.M., Broenkow, W.W., 1987. VERTEX: carbon cycling in the northeast Pacific. Deep-Sea Res. 34 (2), 267–285.
Mittelstaedt, E., 1991. The ocean boundary along the northwest African coast. Prog. Oceanogr. 26, 307–355.
Morita, R.Y., 1984. Feast or famine in the deep sea. Developments in industrial microbiology. Soc. Int. Microbiol. 25, 5–16.
Nagata, T., Fukuda, H., Fukuda, R., Koike, I., 2000. Bacterioplankton distribution and production in the deep Pacific waters: large-scale geographic variations and possible coupling with sinking particle fluxes. Limnol. Oceanogr. 45, 426–435.
Nowald, N., Karakas, G., Ratmeyer, V., Fischer, G., Schlitzer, R., Davenport, R., Wefer, G., 2006. Distribution and transport processes of marine particulate matter off Cape Blanc (NW-Africa): results from vertical camera profiles. Ocean Sci. Discuss. 3, 903–938.
Passow, U., De La Rocha, C., 2006. Accumulation of mineral ballast on organic aggregates. Global Biogeochem. Cycles 20, 1–7.
Ploug, H., Grossart, H.P., 2000. Bacterial growth and grazing on diatom aggregates: respiratory carbon turnover as a function of aggregate size and sinking velocity. Limnol. Oceanogr. 45 (7), 1467–1475.
Ploug, H., Grossart, H.P., Azam, F., Jørgensen, B.B., 1999. Photosynthesis, respiration, and carbon turnover in sinking marine snow from surface waters of Southern California Bight: implications for the carbon cycle in the ocean. Mar. Ecol. Prog. Ser. 179, 1–11.
Ploug, H., Hietanen, S., Kuparinen, J., 2002. Diffusion and advection within and around sinking, porous diatom aggregates. Limnol. Oceanogr. 47 (4), 1129–1136.
Ploug, H., Iversen, M.H., Fischer, G., 2008. Ballast, sinking velocity, and apparent diffusivity within marine snow and zooplankton fecal pellets: implications for substrate turnover by attached bacteria. Limnol. Oceanogr. 53 (5), 1878–1886.
Ploug, H., Jørgensen, B.B., 1999. A net-jet flow system for mass transfer and microsensor studies of sinking aggregates. Mar. Ecol. Prog. Ser. 176, 279–290.
Ploug, H., Kuehl, M., Buchholz-Cleven, B., Jørgensen, B.B., 1997. Anoxic aggregates—an ephemeral phenomenon in the pelagic environment? Aquat. Microb. Ecol. 13 (3) 285–294.
Ploug, H., Terbrüggen, A., Kaufmann, A., Wolf-Gladrow, D., Passow, U., A novel method to measure particle sinking velocity *in vitro*, and its comparison to three other *in vitro* methods. Limnol. Oceanogr. Methods, accepted for publication.
Poulsen, L.K., Iversen, M.H., 2008. Degradation of copepod fecal pellets: key role of protozooplankton. Mar. Ecol. Prog. Ser. 367, 1–13.
Poulsen, L.K., Kiørboe, T., 2005. Coprophagy and coprorhexy in the copepods *Acartia tonas* and *Temora longicornis*: clearance rates and feeding behaviour. Mar. Ecol. Prog. Ser. 299, 217–227.
Ratmeyer, V., Wefer, G., 1996. A high resolution camera system (ParCa) for imaging particles in the ocean: system design and results from profiles and a three-month deployment. J. Mar. Res. 54 (3), 589–603.
Reinthaler, T., van Aken, H., Veth, C., Arístegui, J., Robinson, C., Williams, P.J.L.B., Lebaron, P., Herndl, G.J., 2006. Prokaryotic respiration and production in the meso- and bathypelagic realm of the eastern and western North Atlantic basin. Limnol. Oceanogr. 51, 1262–1273.
Revsbech, N.P., 1989. An oxygen microsensor with a guard cathode. Limnol. Oceanogr. 34, 474–478.
Schlitzer, R., 2000. Applying the adjoint method for biogeochemical modeling: export of particulate organic matter in the world ocean. Inverse Methods Global Biogeochem. Cycles 114, 107–124.
Shanks, A.L., Edmondson, E.W., 1989. Laboratory-made artificial marine snow: a biological model of the real thing. Mar. Biol. 101, 463–470.
Smith, D.C., Simon, M., Alldredge, A.L., Azam, F., 1992. Intense hydrolytic enzyme activity on marine aggregates and implications for rapid particle dissolution. Nature 359 (6391), 139–142.
Steinberg, D.K., 1995. Diet of copepods (Scolpalatum vorax) associated with mesopelagic detritus (giant larvacean houses) in Monterey Bay, California. Mar. Biol. 122, 571–584.
Steinberg, D.K., Silver, M.W., Pilskaln, C.H., Coale, S.L., Paduan, J.B., 1994. Midwater zooplankton communities on pelagic detritus (giant larvacean houses) in Monterey Bay, California. Limnol. Oceanogr. 39 (7), 1606–1620.
Stemmann, L., Gorsky, G., Marty, J.C., Picheral, M., Miquel, J.C., 2002. Four-year study of large-particle vertical distribution (0–1000 m) in the NW Mediterranean in relation to hydrology, phytoplankton, and vertical flux. Deep-Sea Res. II 49 (11), 2143–2162.
Stemmann, L., Jackson, G.A., Gorsky, G., 2004a. A vertical model of particle size distributions and fluxes in the midwater column that includes biological and physical processes. Part II: application to a three year survey in the NW Mediterranean Sea. Deep-Sea Res. I 51 (7), 885–908.
Stemmann, L., Jackson, G.A., Ianson, D., 2004b. A vertical model of particle size distributions and fluxes in the midwater column that includes biological and physical processes. Part I: model formulation. Deep-Sea Res. I 51 (7), 865–884.
Suess, E., 1980. Particulate organic carbon flux in the oceans—surface productivity and oxygen utilization. Nature 288, 260–263.
Van Camp, L., Nykjaer, L., Mittelstaedt, E., Schlittenhardt, P., 1991. Upwelling and boundary circulation off Northwest Africa as depicted by infrared and visible satellite observations. Prog. Oceanogr. 26, 357–402.
Waite, A.M., Nodder, S.D., 2001. The effect of *in situ* addition on the sinking rates and export flux of Southern Ocean diatoms. Deep-Sea Res. II 48, 2635–2654.
Wooster, W.S., Reid, J.L., 1963. Eastern boundary currents. In: Hill, M.N. (Ed.), The Sea II. Interscience, pp. 253–280.